Applied Catalysis B: Environmental 90 (2009) 45–54

Contents lists available at ScienceDirect

Applied Catalysis B: Environmental

journal homepage: www.elsevier.com/locate/apcatb

Water-gas shift reaction over supported Pt-CeO_x catalysts

Yong Tae Kim [a], Eun Duck Park [a,*], Hyun Chul Lee [b], Doohwan Lee [b], Kang Hee Lee [b]

[a] Division of Energy Systems Research and Division of Chemical Engineering and Materials Engineering, Ajou University, Wonchun-Dong Yeongtong-Gu Suwon 443-749, Republic of Korea
[b] Energy and Environment Laboratory, Samsung Advanced Institute of Technology (SAIT), P.O. Box 111, Suwon 440-600, Republic of Korea

ARTICLE INFO

Article history:
Received 26 September 2008
Received in revised form 12 February 2009
Accepted 14 February 2009
Available online 25 February 2009

Keywords:
Water-gas shift
Pt
Ceria
TiO_2
Support
Fuel cell

ABSTRACT

We conducted a comparative study for the water-gas shift (WGS) reaction over ceria-promoted Pt catalysts supported on various supports such as γ-Al_2O_3, SiO_2, TiO_2 (P-25), CeO_2, SiO_2-Al_2O_3, yttria-stabilized zirconia (YSZ) and ZrO_2 in a rather severe reaction condition such as 6.7 vol.% CO, 6.7 vol.% CO_2, and 33.2 vol.% H_2O in H_2. Among them, Pt-Ce/TiO_2 showed the highest WGS activity especially at low temperatures. The effect of preparation sequences on the catalytic activity was also examined for ceria-promoted Pt supported on TiO_2 and Pt-Ce/TiO_2 prepared with a single-step co-impregnation method showed the highest water-gas shift activity. The CO chemisorptions, the temperature-programmed reduction (TPR), an inductively coupled plasma-atomic emission spectroscopy (ICP-AES), and a transmission electron microscopy (TEM) with an energy dispersive X-ray spectroscopy (EDX) were conducted to characterize catalysts. The close correlation between the low-temperature water-gas shift activity and the amounts of chemisorbed CO as well as the degree of interaction between Pt and ceria has been observed. This Pt-Ce/TiO_2 showed the more stable catalytic activity in the cyclic operation and the start-up/shut-down operation compared with the conventional Pt-Ce/CeO_2.

1. Introduction

The fuel processor in which hydrocarbon fuels can be converted into hydrogen has recently attracted much attention as a result of the advancement in the fuel cell technology. In a fuel processor, the water-gas shift (WGS) reaction plays a crucial role in the transformation of CO, a well-known poisonous gas to electrode of fuel cell, into CO_2 through a reaction with steam as follows.

$$CO(g) + H_2O(g) \leftrightarrow CO_2(g) + H_2(g) \quad \Delta H^\circ_{298} = -41,166\,J/mol$$

Because this WGS reaction is exothermic and thermodynamically limited, this has been carried out in a conventional H_2 plant via two-stage processes such as a high-temperature shift (HTS ~ 673 K) and a low-temperature shift (LTS, around 473 K) [1]. Fe-based [2] and Cu-based [3–14] catalyst system has been successfully adopted for each process, respectively. However, these catalyst systems suffer from some drawbacks to be applied to a small-scale fuel processor with characteristics such as a cyclic operation and possibility for air contamination [13–15]. To overcome these weak points of commercial WGS catalysts, some noble metal catalysts including Au and Pt group metals have been extensively studied [16–89]. Supported gold catalysts have received much interest during last decades because of their high WGS activity at low temperatures [16–47]. However, the deactivation phenomena have been considered to be the most important problem to be overcome [40–47]. Panagiotopoulou and Kondarides compared the WGS activity among noble metal catalysts supported on Al_2O_3 and found that the catalytic activity follows the order of Pt > Rh ≈ Ru > Pd [51]. They also found that catalytic activity of Pt and Ru catalysts could be 1–2 order of magnitude higher when supported on "reducible" (TiO_2, CeO_2, La_2O_3, and YSZ) rather than on "irreducible" (Al_2O_3, MgO and SiO_2) metal oxide [51]. The WGS activity following the order of Pt > Rh > Ru ~ Pd > Ir > Au was also reported when supported on ceria-zirconia [74]. Until now, the WGS activity has been measured over Pt-based catalysts supported on various supports such as CeO_2 [47,52–65], ZrO_2 [66–69], $CeZrO_x$ [70–74], $TiZrO_x$ [75], and TiO_2 [77–89]. Among them, Pt/CeO_2 has been frequently reported to be one of active catalysts. However, this catalyst has been reported to be deactivated in the real reformate condition in which the gas stream is composed of 5–7 vol.% CO, 5–7% vol.% CO_2, and 30–40 vol.% H_2O in H_2. The growth in the ceria crystallite size leading to the decrease in the reducibility of large ceria crystallites has been proposed as the cause of deactivation [52]. Liu et al. suggested that deactivation of the Pt/CeO_2 catalysts could be due to the formation of carbonates on the catalyst surface during shut-

* Corresponding author. Tel.: +82 31 219 2384; fax: +82 31 219 1612.
E-mail address: edpark@ajou.ac.kr (E.D. Park).

0926-3373/$ – see front matter © 2009 Elsevier B.V. All rights reserved.
doi:10.1016/j.apcatb.2009.02.011

downs in reformate [55]. To overcome this deactivation problem, two different approaches have been proposed. The one is the additional feed of a small amount of oxygen before the WGS reactor. Deng and Flytzani-Stephanopoulos [47,65] found that the additional oxygen in a feed could oxidize Ce^{III} to Ce^{IV} thus preventing the formation of cerium(III) hydroxycarbonate and that Au-ceria or Pt-ceria catalysts showed the remarkable stability in the WGS reaction in the full fuel-gas mixture both at low and high temperatures and even in a cyclic shut-down/start-up operation. The other approach is to develop the catalyst stable at this severe reaction condition. The addition of MgO to Pt/CeO_2 has been reported to increase the activity and stability of the catalysts via favoring the formate decomposition and lowering the carbonate concentration on the catalyst surface during WGS reaction [60]. The addition of Re into Pt/TiO_2 was also reported to prevent Pt sintering to stabilize the catalytic activity [87,88]. Although various Pt-based catalysts have been examined for the WGS reaction, the low-temperature catalytic activity is still low and the long term catalytic stability has not been successfully accomplished. Recently, the ceria-promoted Pt/TiO_2 catalysts have been reported to show quite promising WGS activity [83,89]. However, the effect of preparation method on the WGS activity has not been examined in detail. Furthermore, the catalytic stability in the cyclic operation over ceria-promoted Pt/TiO_2 has not been reported. In the previous work, we have found that the catalyst prepared with a single-step co-impregnation was more active for the WGS reaction than the catalyst prepared with a sequential impregnation of CeO_x [73]. In this work, the effect of kinds of support and the preparation sequences on the WGS activity has been intensively examined. Furthermore, the catalytic stability in the cyclic operation was also examined, which is quite important for the practical view point.

2. Experimental

2.1. Catalyst preparation and characterization

All the catalysts were prepared with a wet impregnation method from an aqueous solution of $Pt(NH_3)_4(NO_3)_2$ (Aldrich) and $Ce(NO_3)_3{\cdot}6H_2O$ (Junsei). Various supports such as TiO_2 (Degussa, P-25, S_{BET} = 51.3 m^2/g), yttria-stabilized zirconia (YSZ) (Tosoh, TZ-8Y, S_{BET} = 10.7 m^2/g), CeO_2 (Kanto, S_{BET} = 8.9 m^2/g), ZrO_2 (Junsei, S_{BET} = 2.3 m^2/g), SiO_2 (Aldrich, S_{BET} = 348.7 m^2/g), SiO_2-Al_2O_3 (Aldrich, S_{BET} = 549.0 m^2/g), and γ-alumina (Alfa, S_{BET} = 162.0 m^2/g) were purchased and utilized as a support. The content of Pt was intended to be 1 wt.% and the molar ratio between Ce and Pt was intended to be fixed at 5 if not specified explicitly. All the Pt-Ce/support catalysts were prepared with a co-impregnation method. $Pt/Ce/TiO_2$ and $Ce/Pt/TiO_2$ were prepared by a sequential impregnation method with Ce/TiO_2 and Pt/TiO_2 both calcined at 773 K. All the catalysts were calcined at 773 K in air and reduced at 673 K in a hydrogen stream for 1 h before a reaction. As a reference, the commercial Cu-based catalyst such as 36.3% CuO/40.1% ZnO/Al_2O_3 was purchased from Süd-Chemie and utilized for the activity comparison.

Chemical composition of the prepared samples was analyzed by an inductively coupled plasma-atomic emission spectroscopy (ICP-AES, JY-70Plus, Jobin-Yvon), and the results were listed in Table 1.

The BET surface area was calculated from N_2 adsorption data that were obtained using Autosorb-1 apparatus (Quantachrome) at liquid N_2 temperature. Before the measurement, the sample was degassed in vacuum for 4 h at 473 K.

The CO chemisorptions were conducted in an AutoChem 2910 unit (Micromeritics) equipped with a thermal conductivity detector (TCD) to measure CO consumption and an on-line mass spectrometer (QMS 200, Pfeiffer Vacuum) to detect any organic or inorganic species in the effluent stream during CO chemisorptions. Quartz U-tube reactors were generally loaded with 0.1 g of sample, and catalysts were pretreated by reduction in H_2 at 673 K for 1 h, then cooled to room temperature. In the case of supported ceria, the reduction temperature was increased to be 773 K. The CO chemisorptions were carried out at 300 K in 30 ml/min of He stream through a pulsed-chemisorptions technique, in which 500 μl pulses of CO were utilized, after removing any residual hydrogen in a line by flowing He at 300 K for 1 h.

Table 1
The physical properties of prepared catalysts.

Catalysts	BET surface area (m^2/g)	Bulk composition (wt.%)[a]	
		Pt	Ce
Pt-Ce/TiO_2 (Ce/Pt = 5)	48.4	0.87	3.52
Pt-Ce/ZrO_2 (Ce/Pt = 5)	9.4	0.75	2.79
Pt-Ce/YSZ (Ce/Pt = 5)	16.0	0.85	3.3
Pt-Ce/CeO_2 (Ce/Pt = 5)	7.9	0.91	78.7
Pt-Ce/SiO_2 (Ce/Pt = 5)	298.2	0.82	2.50
Pt-Ce/γ-Al_2O_3 (Ce/Pt = 5)	143.0	0.60	2.73
Pt-Ce/SiO_2-Al_2O_3 (Ce/Pt = 5)	435.7	0.85	2.62
Pt/TiO_2	52.7	0.86	–
Ce/Pt/TiO_2 (Ce/Pt = 5)	48.5	0.73	3.05
Pt/Ce/TiO_2 (Ce/Pt = 5)	51.4	0.57	3.02
Pt-Ce/TiO_2 (Ce/Pt = 1)	50.9	0.76	0.63
Pt-Ce/TiO_2 (Ce/Pt = 15)	52.8	0.86	10.0

[a] The bulk composition was analyzed with an ICP-AES.

The modified CO chemisorptions were also carried out in an AutoChem 2910 unit (Micromeritics) equipped with a thermal conductivity detector following the procedure proposed by Takeguchi et al. [90]. The modified CO chemisorptions proceeded on O_2–CO_2–H_2–CO pulse method. Oxygen was fed to the sample at 30 ml/min during programmed heating to 773 K for 2 h. The sample was cooled down to room temperature and was flushed with He for 5 min. Catalysts were treated by reduction in 10%H_2/Ar at 673 K for 1 h, then cooled to room temperature. After the sample was cooled down to room temperature, the sample was flushed with He for 30 min and was exposed to O_2 gas for 10 min. Carbon dioxide was fed to the sample for 10 min, and then the sample was purged with He fed for 10 min. 10% H_2/Ar gas was fed to the sample for 10 min, and the then sample was purged with He gas fed for 30 min. The CO chemisorptions were carried out at 300 K in 30 ml/min of He stream through a pulsed-chemisorptions technique, in which 500 μl pulses of CO were utilized.

Temperature-programmed reduction (TPR) was conducted on in an AutoChem 2910 unit (Micromeritics) equipped with a thermal conductivity detector to measure H_2 consumption and an on-line mass spectrometer (QMS 200, Pfeiffer Vacuum) to detect any organic or inorganic species in the effluent stream during TPR experiment. A water trap composed of blue silica gel removed moisture from the TPR effluent stream at 273 K before the TCD. The reduction of Ag_2O was used to calibrate the TCD signal for H_2 consumption. Quartz U-tube reactors were generally loaded with 0.1 g of sample, and catalysts were pretreated by calcinations in 20 vol.% O_2 in N_2 at 773 K for 1 h, then cooled to room temperature. The TPR was performed using 30 ml/min of 10 vol.% H_2/Ar from 313 to 1173 K at a heating rate of 10 K/min monitoring the thermal conductive detector (TCD) signals after removing any residual oxygen in a line by flowing He at 313 K for 1 h.

The field emission transmission electron microscopy (FE-TEM, Technai F30UT) with a high-angle annular dark-field detector (HAADF) and an energy-dispersive X-ray analyzer (EDX) was operated at 200 kV to monitor the surface morphology and composition of the samples. The TEM image resolution was 0.14 nm. The EDS nanoprobe size was 0.5 nm and the point resolution was 0.17 nm.

2.2. Catalytic performance tests

The catalytic activity was measured in a small fixed bed reactor with catalysts that had been retained between 45 and 80 mesh sieves. For screening tests, a standard gas of 6.7 vol.% CO, 6.7 vol.% CO_2 and 33.2 vol.% H_2O balanced with H_2 was fed to the reactor, in which 0.10 g of catalyst without diluents was contacted with a reactant gas at a flow rate of 150 ml/min, at an atmospheric pressure. The catalytic activity was measured with a ramping rate of 0.39 K/min. The effluent from the reactor passed through the condenser to remove the water vapor and was analyzed by gas chromatograph (HP5890A, Carbosphere column) to determine CO conversion.

For the stability test in the cyclic operation, a standard gas of 6.3 vol.% CO, 6.3 vol.% CO_2, and 37.5 vol.% H_2O in balanced H_2 was fed to the reactor, in which 2.5 g of catalyst without diluents was contacted with a reactant gas at a flow rate of 250 ml/min, at an atmospheric pressure. The catalytic activity was measured with a ramping rate of 1 K/min from 423 to 623 K. The start-up/shut-down cyclic operation was conducted by cycling the following procedure. The steady WGS activity was monitored at 573 K for 10 h followed by the shut-down in a feed to room temperature. In this case, the effluent from the reactor passed through the condenser to remove the water vapor and the dry effluent gas composition was determined on an on-line gas analyzer (NGA2000, MLT4, Rosemount Analyzer System from Emerson Process Management) of each gas components at % level.

3. Results and discussion

The effect of supports on the WGS activity was examined over Pt-Ce catalysts supported on various supports prepared with a single-step co-impregnation method at different reaction temperatures as shown in Fig. 1. Generally, the CO conversion increased with increasing reaction temperatures and then decreased with further increasing reaction temperatures because the WGS reaction is thermodynamically limited. Therefore, the equilibrium CO conversion can be achieved at high temperatures. At kinetically controlled reaction temperature, the WGS activity decreased in the following order: Pt-Ce/TiO_2 > Pt-Ce/YSZ > Pt-Ce/CeO_2 > Pt-Ce/ZrO_2 ~ Pt-Ce/γ-Al_2O_3 ~ Pt-Ce/SiO_2 ≫ Pt-Ce/SiO_2-Al_2O_3. Pt-Ce/CeO_2 showed the similar WGS activity with Pt-Ce/γ-Al_2O_3, Pt-Ce/ZrO_2 and Pt-Ce/SiO_2 below 550 K but its WGS activity increased further to be higher than those of the latter catalysts above 550 K. In the case of Pt-Ce catalyst supported on silica-alumina, no noticeable WGS activity was observed for all reaction temperatures below 673 K. This result implies that the kinds of support can play an important role for the WGS reaction. At the same reaction condition, the support itself did not show any detectable CO conversion during WGS reaction for all reaction temperatures. Various chemisorptions experiments were conducted for supported Pt-Ce catalysts and listed in Table 2. The CO chemisorptions can give us the number of CO adsorption sites including Pt metal and reducible metal oxides. In the case of Pt-Ce/TiO_2, the amount of chemisorbed CO appeared to exceed the number of Pt atom present in the catalyst. This result might imply that CO can be chemisorbed on reduced ceria as well as Pt metal. There can be two possible forms in ceria in Pt-Ce/TiO_2. The one can be located near Pt and the other can be isolated ceria. The former can be easily reduced by hydrogen atom dissociated on Pt metal. The possibility that the isolated ceria can take part in the CO chemisorptions can be checked by the separate CO chemisorptions experiment on reduced Ce/TiO_2. In the case of 3.6 wt.% Ce/TiO_2 after reduced at 773 K, no detectable CO was chemisorbed. Therefore, it can be said that CO chemisorbed on Pt metal and reduced ceria near Pt metal not on isolated reduced ceria in Pt-Ce/TiO_2. Takeguchi et al. [90] proposed the O_2–CO_2–H_2–CO pulse method which is called modified CO chemisorptions in this work to determine the precious metal dispersion on CeO_2-containing catalysts because the supports themselves might adsorb CO. This modified CO chemisorptions were also conducted for all catalysts and listed in Table 2. Compared with those of CO chemisorptions, the amount of chemisorbed CO determined through the modified

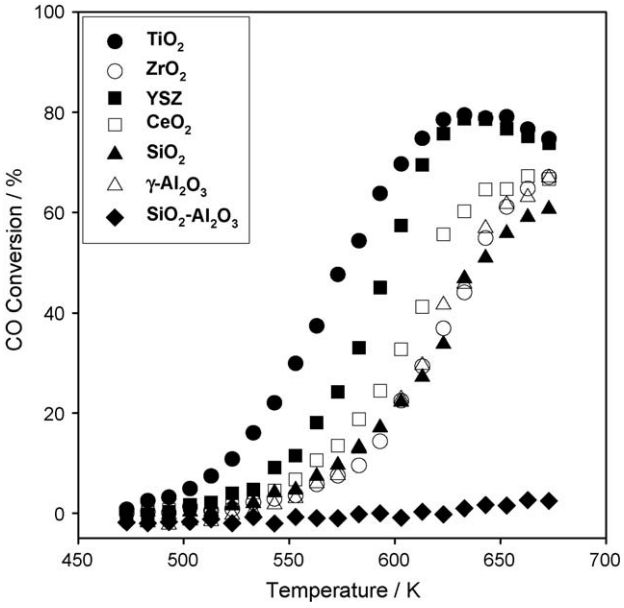

Fig. 1. The CO conversion over 1 wt.% Pt-Ce/support (Ce/Pt = 5) with increasing reaction temperature. The feed composition: 6.7 vol.% CO, 6.7 vol.% CO_2, 33.2 vol.% H_2O in H_2. F/W = 1500 ml/min/g_{cat}.

Table 2
The chemisorption data and the reaction rate at 553 K for supported Pt-Ce catalysts.

Catalysts	CO chemisorption		Modified CO chemisorption		Reaction rate at 553 K ($mol_{CO}\ mol_{Pt}^{-1}\ s^{-1}$)	Normalized reaction rate at 553 K[a] (s^{-1})	Turnover frequency at 553 K[b] (s^{-1})
	CO uptake (μmol/g_{cat})	CO/Pt (%)	CO uptake (μmol/g_{cat})	CO/Pt (%)			
Pt-Ce/TiO_2 (Ce/Pt = 5)	50.0	112.1	35.3	79.2	0.50	0.45	0.63
Pt-Ce/ZrO_2 (Ce/Pt = 5)	6.5	16.9	6.9	17.9	0.07	0.42	0.39
Pt-Ce/YSZ (Ce/Pt = 5)	24.8	56.9	22.2	50.9	0.23	0.41	0.45
Pt-Ce/CeO_2 (Ce/Pt = 5)	11.4	24.4	10.4	22.3	0.11	0.44	0.48
Pt-Ce/SiO_2 (Ce/Pt = 5)	16.4	39.0	9.4	22.4	0.08	0.21	0.37
Pt-Ce/γ-Al_2O_3 (Ce/Pt = 5)	29.4	95.6	16.4	53.3	0.07	0.07	0.13
Pt-Ce/SiO_2-Al_2O_3 (Ce/Pt = 5)	10.6	24.3	12.6	28.9	~0	~0	~0

[a] The normalized reaction rate was calculated by dividing the reaction rate with the amount of chemisorbed CO based on the CO chemisorption.
[b] The turnover frequency was calculated by dividing the reaction rate with the amount of chemisorbed CO based on the modified CO chemisorption.

CO chemisorptions decreased a little for each catalyst except Pt-Ce/ZrO_2 and Pt-Ce/SiO_2-Al_2O_3. In any cases, the largest amount of chemisorbed CO can be observed for Pt-Ce/TiO_2. As mentioned earlier, there can be two possible forms in ceria in Pt-Ce/TiO_2. The WGS activity was also found to be increased with the amount of chemisorbed CO for Pt-Ce catalysts supported on reducible metal oxides such as Pt-Ce/TiO_2, Pt-Ce/YSZ, Pt-Ce/CeO_2 and Pt-Ce/ZrO_2. The most active catalyst, Pt-Ce/TiO_2, can chemisorb the largest amount of CO. On the other hand, no close correlation can be found between the catalytic activity and the amount of chemisorbed CO for Pt-Ce catalysts supported on irreducible metal oxides such as Pt-Ce/γ-Al_2O_3, Pt-Ce/SiO_2 and Pt-Ce/SiO_2-Al_2O_3.

The effect of support on the WGS activity can be clearly discriminated when the comparison of activity is made based on the amount of chemisorbed CO among supported Pt-Ce catalysts. As displayed in Table 2, the normalized reaction rate of Pt-Ce catalysts supported on reducible metal oxides such as Pt-Ce/TiO_2, Pt-Ce/ZrO_2, Pt-Ce/YSZ and Pt-Ce/CeO_2 is almost same. On the other hand, the normalized reaction rate among Pt-Ce catalysts supported on irreducible metal oxides decreased in the following order: Pt-Ce/SiO_2 > Pt-Ce/γ-Al_2O_3 ≫ Pt-Ce/SiO_2-Al_2O_3. Based on the normalized reaction rates, the reducible metal oxides can be considered to be better as a support than the irreducible metal oxides. The turnover frequencies calculated based on the modified CO chemisorptions for supported Pt-Ce catalysts were also compared in Table 2. Pt-Ce/TiO_2 showed the highest turnover frequency among tested catalysts.

At the same reaction condition, the specific activity for the water-gas shift reaction over Pt-Ce/TiO_2 and the commercial Cu-Zn-Al_2O_3 were determined to be 22.3 and 39.2 $\mu mol_{CO}\ g_{cat}^{-1}\ s^{-1}$, respectively. Although the former catalyst showed the less specific activity than the latter one, the former catalyst appeared to be superior to other previous Pt-based catalysts such as 1% Pt/$Ce_{0.75}Zr_{0.25}O_2$ [70] and 2.1% Pt/$Ce_{0.6}Zr_{0.4}O_2$ [74] based on the specific activity based on the amount of Pt in the catalysts at 553 K.

The temperature-programmed reduction with H_2 was carried out to probe the reducibility of prepared catalysts as shown in Fig. 2. The TPR peaks can be divided into two parts for each sample. The low-temperature TPR (LTR) peak, which can be observed from 313 to 473 K, is due to the reduction of ceria near Pt metal and the high-temperature TPR (HTR) peak, which can be obtained above 473 K, is caused by the reduction of isolated ceria on the catalyst [91]. The reduction temperature can be affected by various factors such as the degree of interaction between Pt and ceria, the crystalline size of ceria and the degree of interaction between ceria and the support. The peak position and its intensity which corresponds to the amount of consumed H_2 at LTR region can reveal the degree of interaction of Pt and ceria on the catalyst. Most of ceria on the surface were determined to be reduced at low temperature in the active catalysts. This implies that the intimate contact between Pt and ceria can be important for the high WGS activity for supported Pt-Ce catalysts.

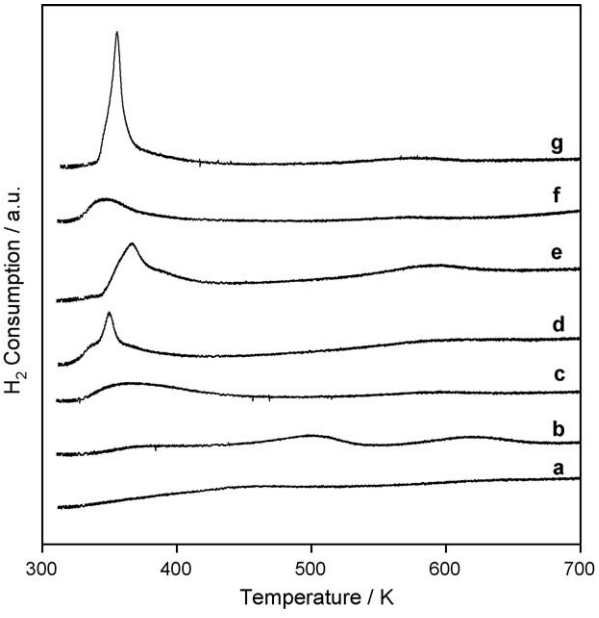

Fig. 2. The TPR patterns of supported Pt-Ce catalysts (Ce/Pt = 5) calcined in air at 773 K. Pt-Ce/SiO_2-Al_2O_3 (a), Pt-Ce/γ-Al_2O_3 (b), Pt-Ce/SiO_2 (c), Pt-Ce/CeO_2 (d), Pt-Ce/YSZ (e), Pt-Ce/ZrO_2 (f), Pt-Ce/TiO_2 (g).

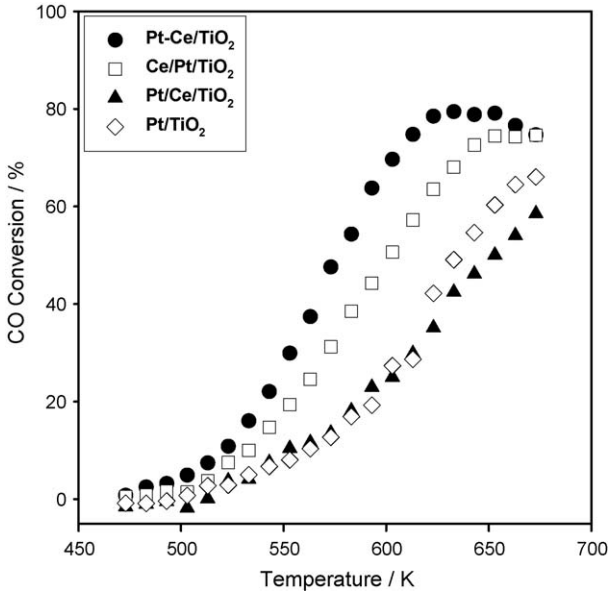

Fig. 3. The CO conversion over Pt/TiO_2 and ceria-promoted Pt/TiO_2 (Ce/Pt = 5) with increasing reaction temperature. The feed composition: 6.7 vol.% CO, 6.7 vol.% CO_2, 33.2 vol.% H_2O in H_2. F/W = 1500 ml/min/g_{cat}.

The effect of the preparation sequence of Pt and ceria in ceria-promoted Pt/TiO_2 on the WGS activity was examined as shown in Fig. 3. As mentioned earlier, the CO conversion generally increased with increasing reaction temperatures and then decreased with further increasing reaction temperatures because the WGS reaction is thermodynamically limited. Therefore, the equilibrium CO conversion can be achieved at high temperatures. At kinetically controlled reaction temperature, the WGS activity decreased in the following order: Pt-Ce/TiO_2 > Ce/Pt/TiO_2 > Pt/TiO_2 ~ Pt/Ce/TiO_2. Interestingly, the WGS activity was strongly dependent on the preparation sequence. The amount of chemisorbed CO was summarized in Table 3 with the reaction rate at 553 K. The most active Pt-Ce/TiO_2 catalyst also showed the largest amount of chemisorbed CO. When the normalized reaction rates, which were calculated by dividing the reaction rate with the amount of chemisorbed CO for Pt/TiO_2 and ceria-promoted Pt/TiO_2, were compared, Ce/Pt/TiO_2 showed the largest value among them. On the other hand, the similar turnover frequencies can be obtained for Ce/Pt/TiO_2 and Pt-Ce/TiO_2. Based on these results, the enhanced WGS activity of Pt-Ce/TiO_2 can be due to the enrichment of active sites for CO chemisorptions.

The effect of the molar ratio between Ce and Pt over Pt-Ce/TiO_2 on the WGS activity was examined as shown in Fig. 4. As mentioned earlier, the CO conversion generally increased with increasing reaction temperatures and then decreased with further increasing reaction temperatures because the WGS reaction is thermodynamically limited. Therefore, the equilibrium CO conversion can be achieved at high temperatures. At kinetically

Table 3
The chemisorption data and the reaction rate at 553 K for Pt/TiO_2 and ceria-promoted Pt/TiO_2 catalysts.

Catalysts	CO chemisorption		Modified CO chemisorption		Reaction rate at 553 K ($mol_{CO}\ mol_{Pt}^{-1}\ s^{-1}$)	Normalized reaction rate at 553 K[a] (s^{-1})	Turnover frequency at 553 K[b] (s^{-1})
	CO uptake ($\mu mol/g_{cat}$)	CO/Pt (%)	CO uptake ($\mu mol/g_{cat}$)	CO/Pt (%)			
Pt/TiO_2	11.5	26.1	13.5	30.8	0.14	0.52	0.44
$Ce/Pt/TiO_2$ (Ce/Pt = 5)	20.4	54.5	22.0	58.8	0.38	0.71	0.65
$Pt/Ce/TiO_2$ (Ce/Pt = 5)	18.3	62.6	20.3	69.5	0.26	0.42	0.38
$Pt\text{-}Ce/TiO_2$ (Ce/Pt = 5)	50.0	112.1	35.3	79.2	0.50	0.45	0.63

[a] The normalized reaction rate was calculated by dividing the reaction rate with the amount of chemisorbed CO based on the CO chemisorption.
[b] The turnover frequency was calculated by dividing the reaction rate with the amount of chemisorbed CO based on the modified CO chemisorption.

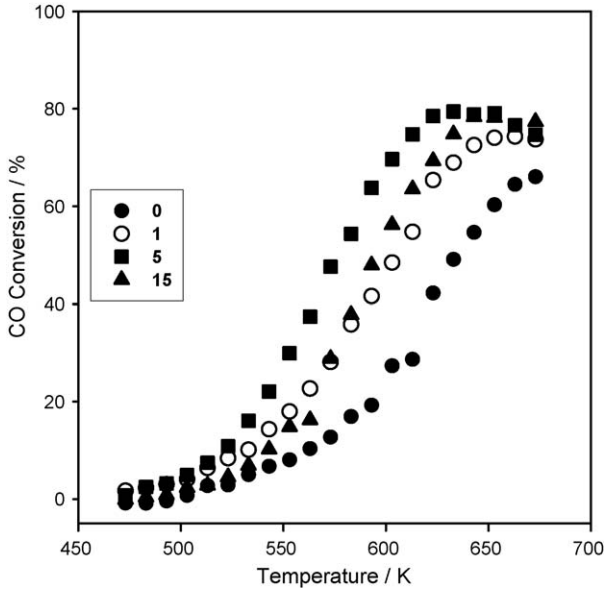

Fig. 4. The CO conversion over $Pt\text{-}Ce/TiO_2$ catalysts containing different amount of Ce/Pt with increasing reaction temperature. The feed composition: 6.7 vol.% CO, 6.7 vol.% CO_2, 33.2 vol.% H_2O in H_2. F/W = 1500 ml/min/g_{cat}.

controlled reaction temperature, the WGS activity increased, showed the maximum value and then decreased with increasing Ce/Pt. The maximum activity was observed when the Ce/Pt was 5.

The temperature-programmed reduction with H_2 were conducted to find out the effect of the preparation sequence of Pt and ceria in ceria-promoted Pt/TiO_2 and the effect of the molar ratio between Ce and Pt over $Pt\text{-}Ce/TiO_2$ on the reducibility as displayed in Fig. 5. Two distinct TPR peaks can be found over $Ce/Pt/TiO_2$ at 414 and 578 K, respectively. $Pt/Ce/TiO_2$ has also two separate peaks at 410 and 570 K, respectively. In the case of $Pt\text{-}Ce/TiO_2$, a strong peak was obtained at 356 K and a weak peak was also observed at 577 K. As mentioned earlier, the TPR peak at low temperatures is due to the reduction of CeO_x near Pt metal and the TPR peak at high temperatures is caused by the reduction of the isolated ceria on the support [91]. The presence of very weak TPR peak at high temperatures over $Pt\text{-}Ce/TiO_2$ implies that most of ceria species are located near Pt metal. The TPR peak at the lowest temperature observed over $Pt\text{-}Ce/TiO_2$ also supports that the intimate contact between Pt and ceria can be made in the catalyst preparation step. The most active catalyst, $Pt\text{-}Ce/TiO_2$, showed the largest LTR peak at the lowest temperature.

In the case of Pt/TiO_2, two broad TPR peaks were obtained at 366 and 537 K over which can be due to the reduction of PtO interacting with support differently. Two distinct peaks were observed at 364 and 539 K over $Pt\text{-}Ce/TiO_2$ (Ce/Pt = 1). In the case of $Pt\text{-}Ce/TiO_2$ (Ce/Pt = 15), a sharp peak with a shoulder was obtained at 387 K and the two broad peaks were also observed at 577 and 939 K. The TPR peak at 939 K can be due to the reduction of bulk ceria which was also observed in the TPR pattern of CeO_2. It was found that ceria could be easily reduced on TiO_2 support compared with the TPR pattern of ceria itself. However, the TPR peaks of Ce/TiO_2 were located at higher temperatures compared with those of ceria-promoted Pt/TiO_2, which implied that ceria can be reduced easily in the presence of Pt metal.

These TPR peaks of Pt/TiO_2 and ceria-promoted Pt/TiO_2 were analyzed and summarized in Table 4. The most active $Pt\text{-}Ce/TiO_2$ showed the largest reduced fraction at the lowest temperature,

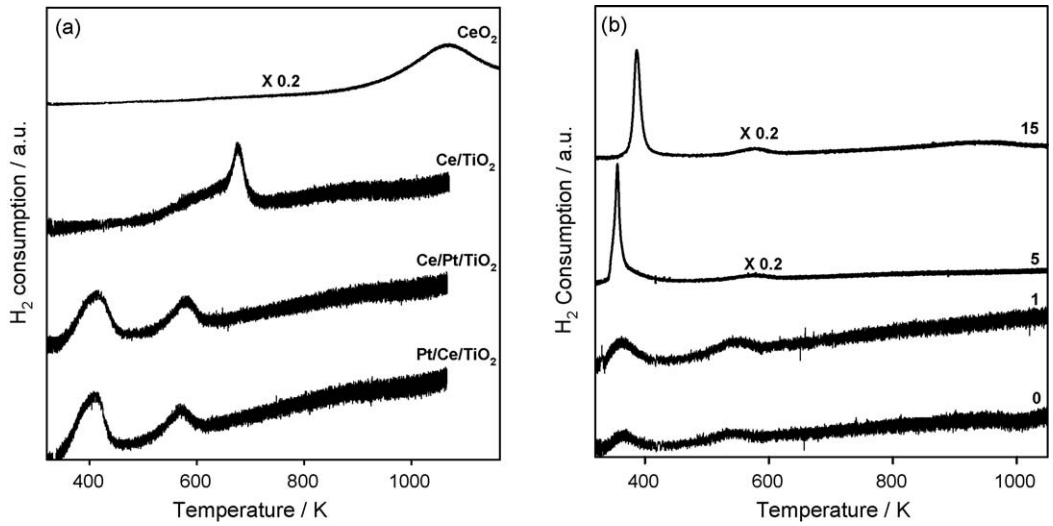

Fig. 5. The TPR patterns of (a) $Pt/Ce/TiO_2$ (Ce/Pt = 5), $Ce/Pt/TiO_2$ (Ce/Pt = 5), 3.6 wt.% Ce/TiO_2, and CeO_2 and (b) $Pt\text{-}Ce/TiO_2$ catalysts containing the different amount of Ce/Pt.

Table 4
The low-temperature TPR peak analysis for Pt/TiO_2 and ceria-promoted Pt/TiO_2 catalysts.

Catalysts	Peak position (K)	H_2 consumption ($\mu mol/g_{cat}$)	Reduced fraction[a] (%)
Pt/TiO_2	366.0	19.0	43.1
$Ce/Pt/TiO_2$ (Ce/Pt = 5)	414.2	58.3	39.9
$Pt/Ce/TiO_2$ (Ce/Pt = 5)	410.5	63.2	46.1
$Pt\text{-}Ce/TiO_2$ (Ce/Pt = 5)	355.7	143.0	84.0
$Pt\text{-}Ce/TiO_2$ (Ce/Pt = 1)	364.4	20.3	33.1
$Pt\text{-}Ce/TiO_2$ (Ce/Pt = 15)	387.2	141.8	35.3

[a] The reduced fraction is defined by dividing the amount of the consumed hydrogen from 313 to 473 K with the theoretical total amount of hydrogen required to convert Ce^{4+} and Pt^{2+} into Ce^{3+} and Pt^0 in the catalysts.

which can be interpreted that the most intimate contact can be made for this catalyst between Pt and ceria. This is consistent with the conclusion derived from chemisorptions data.

The morphology of Pt metals on TiO_2 in the Pt/TiO_2, $Pt/Ce/TiO_2$, $Ce/Pt/TiO_2$, and $Pt\text{-}Ce/TiO_2$ can be observed with the transmission electron microscopy (TEM) as shown in Fig. 6. Some nanoparticles around 2 nm can be found on support in the bright-field TEM image. The particle size distribution of Pt metals was obtained by counting more than 200 particles and the average metallic particle size was determined to be 1.6 ± 0.5, 2.0 ± 1.1, 2.1 ± 0.8, and 2.1 ± 0.6 nm for Pt/TiO_2, $Pt/Ce/TiO_2$, $Ce/Pt/TiO_2$, and $Pt\text{-}Ce/TiO_2$ based on the TEM images as shown in Fig. 6. The metal particle size was smaller in the absence of ceria compared with the case in the presence of ceria. No noticeable difference in the average particle sizes of metals can be observed among ceria-promoted Pt/TiO_2 catalysts. Based on the TEM image, the presence of ceria cannot be confirmed. No separate ceria patch can be observed. Therefore, the energy dispersive X-ray analyzer (EDX) was carried out to find out the presence of Ce in the specific point in the $Pt\text{-}Ce/TiO_2$ (Ce/Pt = 5) catalyst. Three representative points, in which the distinct nanoparticles were observed, were selected for the EDX analysis as shown in Fig. 7. In all points, the presence of Ce and Pt was confirmed. This result supports that ceria is present near Pt metal.

The stability test was conducted over $Pt\text{-}Ce/TiO_2$ catalyst at 633 K as shown in Fig. 8. For comparison, Pt/TiO_2 catalyst was also tested at the same reaction condition. For all reaction data, the reaction condition was chosen for the CO conversion to be smaller than the equilibrium conversion. To accelerate the catalyst deactivation, the very high space velocity, which was higher than those chosen in most previous works by about 10 times, was adopted in this work. Although $Pt\text{-}Ce/TiO_2$ showed the slowly decreasing WGS activity in the continuous operation, this catalyst can be regarded as the more stable compared with Pt/TiO_2 because the latter catalyst showed the rapid decreasing WGS activity with time on stream. Azzam et al. observed the same deactivation phenomena over Pt/TiO_2 and explained it by the loss of Pt surface area which could be due to the presence of traces of formaldehyde formed under WGS reaction conditions by reaction of H_2 and CO [85]. As pointed out by Deng and Flytzani-Stephanopoulos, the cyclic operation including the start-up/shut-down operation is much severer reaction condition for the WGS catalyst than the continuous operation [47]. Therefore, the catalyst stability was examined over $Pt\text{-}Ce/TiO_2$ in the cyclic operation from 423 to 623 K as displayed in Fig. 9. During 10 cycles, the stable catalytic performance can be achieved. This catalyst was also tested in the start-up/shut-down operation as shown in Fig. 10. The stable catalytic performance in the WGS activity can be obtained. On the other hand, the rapid deactivation occurred over $Pt\text{-}Ce/CeO_2$ as shown in Fig. 11. The TEM images were obtained for $Pt\text{-}Ce/TiO_2$ after the start-up/shut-down operation and the same catalyst after the cyclic operation as shown in Fig. 12. The average metallic particle size was determined to be 1.9 ± 0.7 and 2.5 ± 0.7 nm for $Pt\text{-}Ce/TiO_2$ after the start-up/shut-down operation and the same catalyst after the cyclic operation, respectively. The particle size of metals appeared to be increased after the cyclic operation. On the other hand, the particle size of metals was maintained even after start-up/shut-down operation. The CO chemisorptions was also conducted for Pt/TiO_2 and ceria-promoted Pt/TiO_2 after a reaction in a different condition and listed in Table 5. Compared with those of fresh catalysts, the amounts of chemisorbed CO were determined to be decreased for each catalyst after a reaction in a different degree

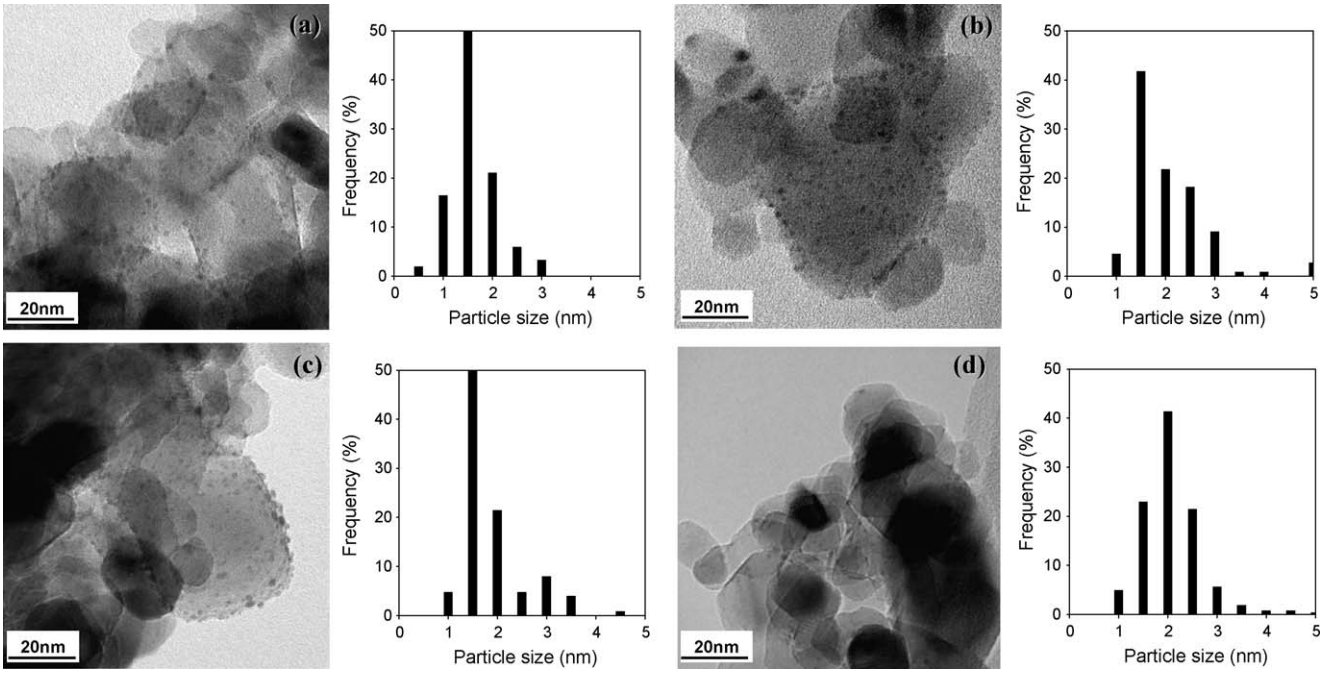

Fig. 6. The TEM images and the particle size distribution of Pt metals in Pt/TiO_2 and ceria-promoted Pt/TiO_2 (Ce/Pt = 5) catalysts. Pt/TiO_2 (a), $Ce/Pt/TiO_2$ (b), $Pt/Ce/TiO_2$ (c), $Pt\text{-}Ce/TiO_2$ (d).

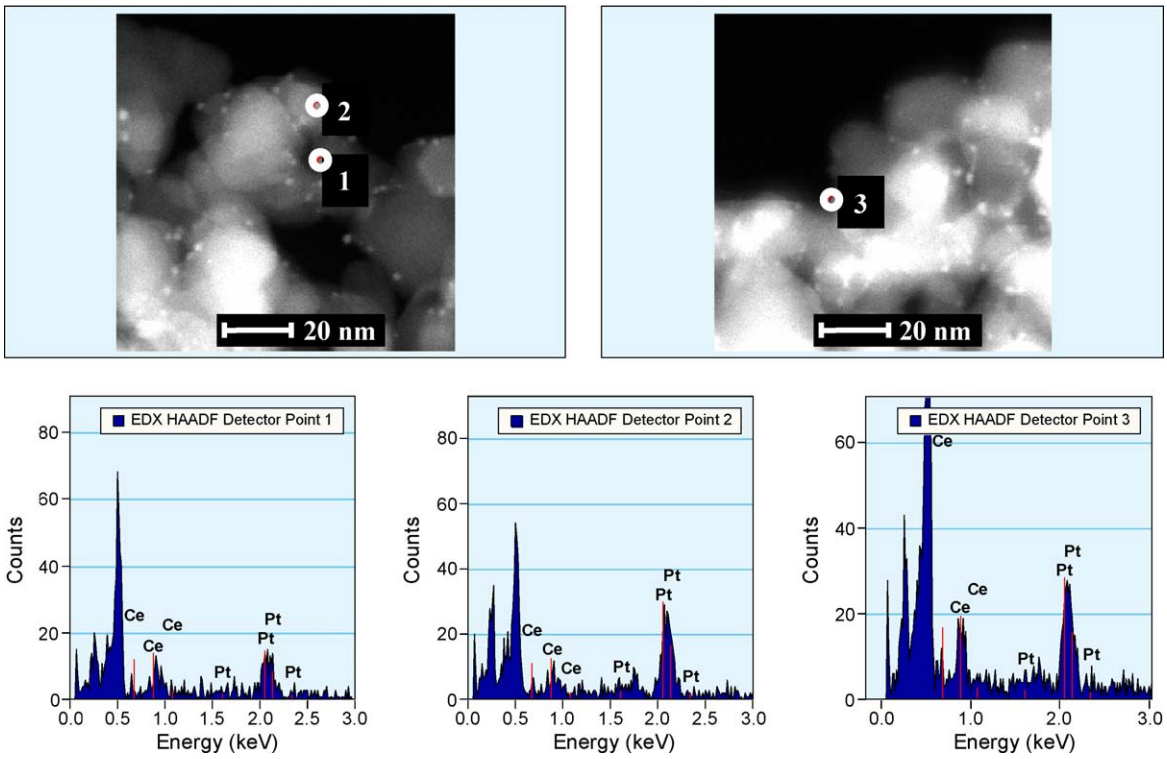

Fig. 7. The EDX analysis at different points in Pt-Ce/TiO_2 (Ce/Pt = 5).

depending on the reaction condition. In the case of Pt/TiO_2, the noticeable decrease in the amount of chemisorbed CO determined by both the CO chemisorptions and the modified CO chemisorptions was observed. On the other hand, the amount of chemisorbed CO decreased in the similar degree for Pt-Ce/TiO_2 during a reaction. Based on CO chemisorptions data, the sintering of Pt metal on TiO_2 can be supported, which has been already reported by Azzam et al. [85]. On the other hand, no distinct agglomeration of metal particles can be observed based on TEM images over Pt-Ce/TiO_2 catalysts after start-up/shut-down operation. The ceria near Pt can stabilize the Pt metal not to be sintered. Instead, the amounts of chemisorbed CO appeared to be decreased after a reaction, which implied that the interaction between Pt and ceria might be weakened during a reaction.

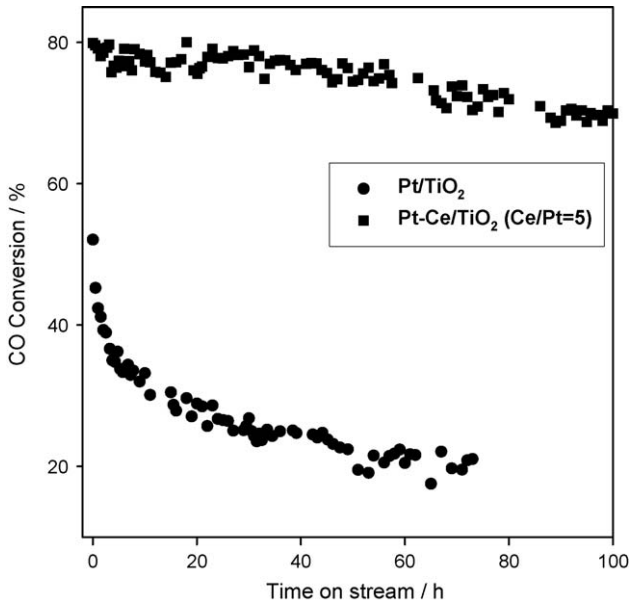

Fig. 8. The stability test at 633 K over Pt/TiO_2 and Pt-Ce/TiO_2 (Ce/Pt = 5) with time on stream. The feed composition: 6.7 vol.% CO, 6.7 vol.% CO_2, 33.2 vol.% H_2O in H_2. F/W = 1500 ml/min/g_{cat}.

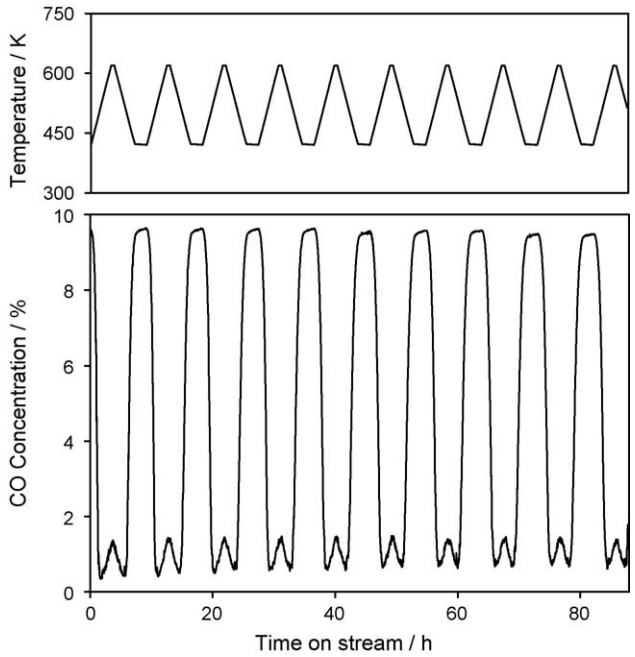

Fig. 9. The thermal cyclic test of Pt-Ce/TiO_2 (Ce/Pt = 5) for water-gas shift reaction. The feed composition: 6.3 vol.% CO, 6.3 vol.% CO_2, 37.5 vol.% H_2O in H_2. F/W = 100 ml/min/g_{cat}.

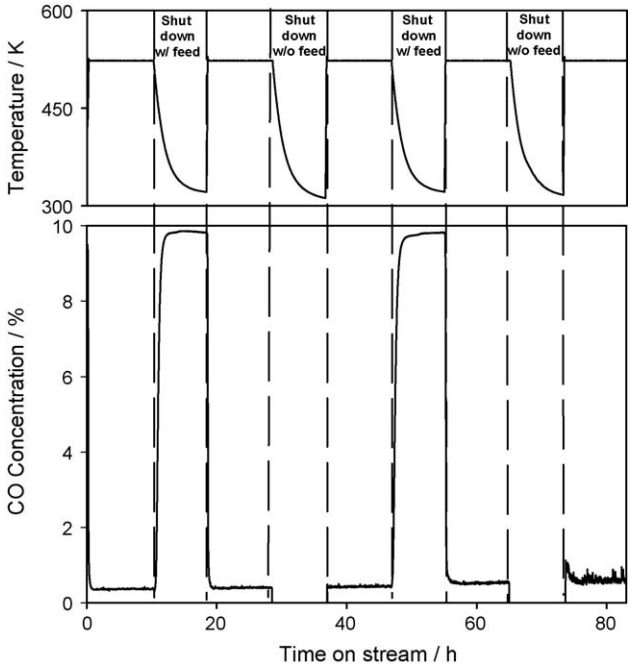

Fig. 10. The start-up/shut-down test of Pt-Ce/TiO_2 (Ce/Pt = 5) for water-gas shift reaction. The feed composition: 6.3 vol.% CO, 6.3 vol.% CO_2, 37.5 vol.% H_2O in H_2. F/W = 100 ml/min/g_{cat}.

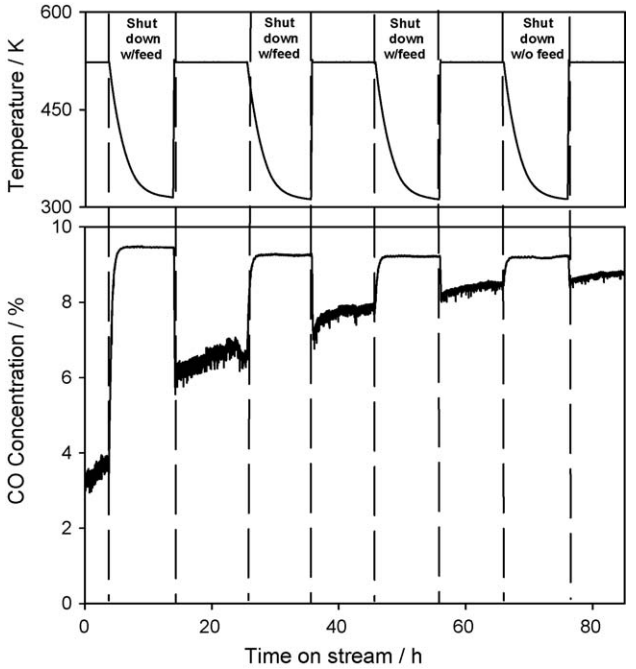

Fig. 11. The start-up/shut-down test of Pt-Ce/CeO_2 (Ce/Pt = 10) for water-gas shift reaction. The feed composition: 6.3 vol.% CO, 6.3 vol.% CO_2, 37.5 vol.% H_2O in H_2. F/W = 100 ml/min/g_{cat}.

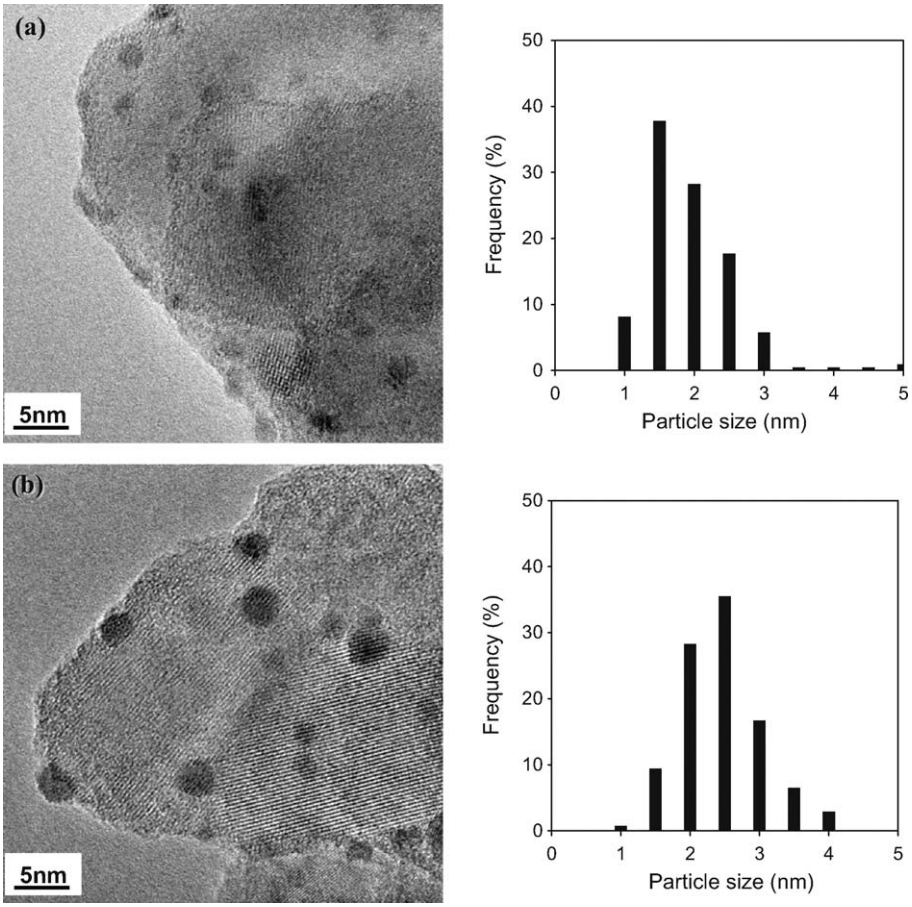

Fig. 12. The TEM images and the particle size distribution of Pt metals in Pt-Ce/TiO_2 (Ce/Pt = 5) after start-up/shut-down test (a) or after thermal cyclic test (b).

Table 5
The chemisorption data for Pt/TiO_2 and $Pt\text{-}Ce/TiO_2$ (Ce/Pt = 5) after a reaction.

Catalysts	CO chemisorption		Modified CO chemisorption	
	CO uptake ($\mu mol/g_{cat}$)	CO/Pt (%)	CO uptake ($\mu mol/g_{cat}$)	CO/Pt (%)
Pt/TiO_2 after a reaction at 633 K	4.0	9.1	3.3	7.5
$Pt\text{-}Ce/TiO_2$ after a reaction at 633 K	21.5	48.3	20.1	45.0
$Pt\text{-}Ce/TiO_2$ after a cyclic operation	23.0	51.5	24.4	54.6
$Pt\text{-}Ce/TiO_2$ after a start-up/shut-down operation	46.1	103.3	22.2	49.7

4. Conclusion

Based on the comparison work for the water-gas shift reaction over ceria-promoted Pt catalysts supported on various supports such as $\gamma\text{-}Al_2O_3$, SiO_2, TiO_2 (P-25), CeO_2, $SiO_2\text{-}Al_2O_3$, yttria-stabilized zirconia and ZrO_2 in a rather severe reaction condition such as 6.7 vol.% CO, 6.7 vol.% CO_2, and 33.2 vol.% H_2O in H_2, $Pt\text{-}Ce/TiO_2$ can be selected to show the highest WGS activity especially at low temperatures. $Pt\text{-}Ce/TiO_2$ prepared with a single-step co-impregnation method showed the highest WGS activity among ceria-promoted Pt/TiO_2 catalysts. The close correlation between the low-temperature water-gas shift activity and the amounts of chemisorbed CO as well as the degree of interaction between Pt and ceria has been observed. This $Pt\text{-}Ce/TiO_2$ showed the more stable catalytic activity in the cyclic operation and the start-up/shut-down operation compared with the conventional $Pt\text{-}Ce/CeO_2$.

Acknowledgement

This work was supported by the Korea Research Foundation Grant funded by the Korean Government (MEST) (KRF-2007-412-J04001).

References

[1] M.I. Temkin, Adv. Catal. 28 (1979) 173–291.
[2] D.S. Newsome, Catal. Rev. Sci. Eng. 21 (1980) 275–318.
[3] M.J.L. Ginés, N. Amadeo, M. Laborde, C.R. Apesteguía, Appl. Catal. A: Gen. 131 (1995) 283–296.
[4] T. Shishido, M. Yamamoto, D.L. Li, Y. Tian, H. Morioka, M. Honda, T. Sano, K. Takehira, Appl. Catal. A: Gen. 303 (2006) 62–71.
[5] J.B. Ko, C.M. Bae, Y.S. Jung, D.H. Kim, Catal. Lett. 105 (2005) 157–161.
[6] H. Kušar, S. Hočevar, J. Levec, Appl. Catal. B: Environ. 63 (2006) 194–200.
[7] Y. Li, Q. Fu, M. Flytzani-Stepanopoulos, Appl. Catal. B: Environ. 27 (2000) 179–191.
[8] D.C. Yeragi, N.C. Pradhan, A.K. Dalai, Catal. Lett. 112 (2006) 139–148.
[9] T. Tabakova, V. Idakiev, J. Papavasiliou, G. Avgouropoulos, T. Ioannides, Catal. Commun. 8 (2007) 101–106.
[10] P. Kumar, R. Idem, Energy Fuels 21 (2007) 522–529.
[11] H. Yahiro, K. Murawaki, K. Saiki, T. Yamamoto, H. Yamaura, Catal. Today 126 (2007) 436–440.
[12] F. Huber, H. Meland, M. Røning, H. Venvik, A. Holmen, Top. Catal. 45 (2007) 101–104.
[13] O. Ilinich, W. Ruettinger, X.S. Liu, R. Ferrauto, J. Catal. 247 (2007) 112–118.
[14] M.V. Twigg, M.S. Spencer, Appl. Catal. A: Gen. 212 (2001) 161–174.
[15] T. Giroux, S. Hwang, Y. Liu, W. Ruettinger, L. Shore, Appl. Catal. B: Environ. 56 (2005) 95–110.
[16] G.C. Bond, C. Louis, D.T. Thompson, Catalysis by Gold, vol. 6, Imperial College Press, 2006.
[17] P. Liu, J.A. Rodriguez, J. Chem. Phys. 126 (2007) 164705.
[18] D. Andreeva, Gold Bull. 35 (2002) 82–88.
[19] D. Andreeva, V. Idakiev, T. Tabakova, A. Andreev, J. Catal. 158 (1996) 354–355.
[20] B.A.A. Silberova, M. Makkee, J.A. Moulijn, Top. Catal. 44 (2007) 209–221.
[21] A. Venugopal, M.S. Scurrell, Appl. Catal. A: Gen. 258 (2004) 241–249.
[22] H. Sakurai, A. Ueda, T. Kobayashi, M. Haruta, Chem. Commun. 3 (1997) 271–272.
[23] F. Boccuzzi, A. Chiorino, M. Manzoli, D. Andreeva, T. Tabakova, L. Ilieva, V. Iadakiev, Catal. Today 75 (2002) 169–175.
[24] N. Hammer, I. Kvande, D. Chen, M. Rønning, Catal. Today 122 (2007) 365–369.
[25] W. Deng, C. Carpenter, N. Yi, M. Flytzani-Stephanopoulos, Top. Catal. 44 (2007) 199–208.
[26] D. Andreeva, V. Idakiev, T. Tabakova, L. Ilieva, P. Falaras, A. Bourlinos, A. Travlos, Catal. Today 72 (2002) 51–57.
[27] Q. Fu, H. Saltsburg, M. Flytzani-Stephanopoulos, Science 301 (2003) 935–938.
[28] Q. Fu, W.L. Deng, H. Saltsburg, M. Flytzani-Stephanopoulos, Appl. Catal. B: Environ. 56 (2005) 57–68.
[29] W.L. Deng, J.D. Jesus, H. Saltsburg, M. Flytzani-Stephanopoulous, Appl. Catal. A: Gen. 291 (2005) 126–135.
[30] A. Luengnaruemitchai, S. Osuwan, E. Gulari, Catal. Commun. 4 (2003) 215–221.
[31] C.H. Kim, L.T. Thompson, J. Catal. 244 (2006) 248–250.
[32] R. Si, M. Flytzani-Stephanopoulous, Angew. Chem. Int. Ed. 47 (2008) 2884–2887.
[33] S. Golunski, R. Rajaram, N. Hodge, G.J. Hutchings, C.J. Kiely, Catal. Today 72 (2002) 107–113.
[34] F.C. Meunier, D. Reid, A. Goquet, S. Shekhtman, C. Hardacre, R. Burch, W. Deng, M. Flytzani-Stephanoporous, J. Catal. 247 (2007) 277–287.
[35] A. Karpenko, R. Leppelt, V. Plzak, J. Cai, A. Chuvilin, B. Schumacher, U. Kaiser, R.J. Behm, Top. Catal. 44 (2007) 183–198.
[36] V. Idakiev, T. Tabakova, A. Naydenov, Z.-Y. Yuan, B.-L. Su, Appl. Catal. B: Environ. 63 (2006) 178–186.
[37] M. Manzoli, F. Vindigni, A. Chiorino, T. Tabakova, V. Idakiev, F. Boccuzzi, React. Kinet. Catal. Lett. 91 (2007) 213–221.
[38] T. Tabakova, V. Idakiev, D. Andreeva, I. Mitov, Appl. Catal. A: Gen. 202 (2000) 91–97.
[39] C.T. Campbell, Science 306 (2004) 234–235.
[40] C.H. Kim, L.T. Thompson, J. Catal. 230 (2005) 66–74.
[41] R. Leppelt, B. Schumacher, V. Plzak, M. Kinne, R.J. Behm, J. Catal. 244 (2006) 137–152.
[42] Y. Denkwitz, A. Karpenko, V. Plzak, R. Leppelt, B. Schumacher, R.J. Behm, J. Catal. 246 (2007) 74–90.
[43] A. Karpenko, R. Leppelt, J. Cai, V. Plzak, A. Chuvilin, U. Kaiser, R.J. Behm, J. Catal. 250 (2007) 139–150.
[44] A.A. Fonseca, J.M. Fisher, D. Ozkaya, M.D. Shannon, D. Thompsett, Top. Catal. 44 (2007) 223–235.
[45] D. Tibiletti, A. Amieiro-Fonseca, R. Burch, Y. Chen, J.M. Fisher, A. Goguet, C. Hardacre, P. Hu, D. Thompsett, J. Phys. Chem. B 109 (2005) 22553–22559.
[46] A. Goguet, R. Burch, Y. Chen, C. Hardacre, P. Hu, R.W. Joyner, F.C. Meunier, B.S. Mun, D. Thompsett, D. Tibiletti, J. Phys. Chem. C 111 (2007) 16927–16933.
[47] W.L. Deng, M. Flytzani-Stephanopoulos, Angew. Chem. 118 (2006) 2343–2347.
[48] S. Hilaire, X. Wang, T. Luo, R.J. Gorte, J. Wagner, Appl. Catal. A: Gen. 215 (2001) 271–278.
[49] A. Basińska, L. Kepiński, F. Domka, Appl. Catal. A: Gen. 183 (1999) 143–153.
[50] G. Jacobs, E. Chenu, P.M. Patterson, L. Williams, D. Sparks, G. Thomas, B.H. Davis, Appl. Catal. A: Gen. 258 (2004) 203–214.
[51] P. Panagiotopoulou, D.I. Kondarides, Catal. Today 112 (2006) 49–52.
[52] T. Bunluesin, R.J. Gorte, G.W. Graham, Appl. Catal. B: Environ. 15 (1998) 107–114.
[53] G. Jacobs, A. Crawford, L. Williams, P.M. Patterson, B.H. Davis, Appl. Catal. A: Gen. 267 (2004) 27–33.
[54] G. Jacobs, P.M. Patterson, U.M. Graham, D.E. Sparks, B.H. Davis, Appl. Catal. A: Gen. 269 (2004) 63–73.
[55] X.H. Liu, W. Ruettinger, X. Xu, R. Farrauto, Appl. Catal. B: Environ. 56 (2005) 69–75.
[56] G. Jacobs, U.M. Graham, E. Chenu, P.M. Patterson, A. Dozier, B.H. Davis, J. Catal. 229 (2005) 499–512.
[57] R.J. Gorte, S. Zhao, Catal. Today 104 (2005) 18–24.
[58] C.M.Y. Yeung, F. Meunier, R. Burch, D. Thompsett, S.C. Tsang, J. Phys. Chem. B 110 (2006) 8540–8543.
[59] C.M.Y. Yeung, K.M.K. Yu, Q.J. Fu, D. Thompsett, M.I. Petch, S.C. Tsang, J. Am. Chem. Soc. 127 (2005) 18010–18011.
[60] A.M.D. Farias, A.P.M.G. Barandas, R.F. Perez, M.A. Fraga, J. Power Sources 165 (2007) 854–860.
[61] C. Zerva, C.J. Philippopoulos, Appl. Catal. B: Environ. 67 (2006) 105–112.
[62] P. Bera, S. Malwadkar, A. Gayen, C.V.V. Satyanarayana, B.S. Rao, M.S. Hegde, Catal. Lett. 96 (2004) 213–219.
[63] P. Panagiotopoulou, J. Papavasiliou, G. Avgouropoulos, T. Ioannides, D.I. Kondarides, Chem. Eng. J. 134 (2007) 16–22.
[64] H.N. Evin, G. Jacobs, J. Ruiz-Martinez, G.A. Thomas, B.H. Davis, Catal. Lett. 120 (2008) 166–178.
[65] D. Pierre, W.L. Deng, M. Flytzani-Stephanopoulos, Top. Catal. 46 (2007) 363–373.
[66] P.S. Querino, J.R.C. Bispo, M.C. Rangel, Catal. Today 107–108 (2005) 920–925.
[67] D. Tibiletti, F.C. Meunier, A. Goquet, D. Reid, R. Burch, M. Boaro, M. Vicario, A. Trovarelli, J. Catal. 244 (2006) 183–191.
[68] J.M. Pigos, C.J. Brooks, G. Jacobs, B.H. Davis, Appl. Catal. A: Gen. 319 (2007) 47–57.
[69] J.M. Pigos, C.J. Brooks, G. Jacobs, B.H. Davis, Appl. Catal. A: Gen. 328 (2007) 14–26.
[70] S. Ricote, G. Jacobs, M. Milling, Y. Ji, P.M. Patterson, B.H. Davis, Appl. Catal. A: Gen. 303 (2006) 35–47.
[71] R. Radhakrishnan, R.R. Willigan, Z. Dardas, T.H. Vanderspurt, Appl. Catal. B: Environ. 66 (2006) 23–28.
[72] W. Ruettinger, X.H. Liu, R.J. Farrauto, Appl. Catal. B: Environ. 65 (2006) 135–141.
[73] H.C. Lee, D.H. Lee, O.Y. Lim, S.H. Kim, Y.T. Kim, E.Y. Ko, E.D. Park, Stud. Surf. Sci. Catal. 167 (2007) 201–206.
[74] R. Radhakrishnan, R.R. Willigan, Z. Dardas, T.H. Vanderspurt, AIChE J. 52 (2006) 1888–1894.
[75] M. Laniecki, M. Igacik, Catal. Today 116 (2006) 400–407.
[76] N. Schumacher, A. Boisen, S. Dahl, A.A. Gokhale, S. Kandoi, L.C. Grabow, J.A. Dumesic, M. Mavrikakis, I. Chorkendorff, J. Catal. 229 (2005) 265–275.
[77] P. Panagiotopoulou, D.I. Kondarides, J. Catal. 225 (2004) 327–336.
[78] H. Iida, A. Igarashi, Appl. Catal. A: Gen. 303 (2006) 192–198.

[79] H. Iida, A. Igarashi, Appl. Catal. A: Gen. 298 (2006) 152–160.
[80] H. Iida, K. Kondo, A. Igarashi, Catal. Commun. 7 (2006) 240–244.
[81] P. Panagiotopoulou, A. Christodoulakis, D.I. Kondarides, S. Boghosian, J. Catal. 240 (2006) 114–125.
[82] Y. Sato, K. Terada, Y. Soma, T. Miyao, S. Naito, Catal. Commun. 7 (2006) 91–95.
[83] P. Panagiotopoulou, D.I. Kondarides, Catal. Today 127 (2007) 319–329.
[84] O. Thinon, F. Diehl, P. Avenier, Y. Schuurman, Catal. Today 137 (2008) 29–35.
[85] K.G. Azzam, I.V. Babich, K. Seshan, L. Lefferts, Appl. Catal. A: Gen. 338 (2008) 66–71.
[86] K.G. Azzam, I.V. Babich, K. Seshan, L. Lefferts, J. Catal. 251 (2007) 153–162.
[87] K.G. Azzam, I.V. Babich, K. Seshan, L. Lefferts, Appl. Catal. B: Environ. 80 (2008) 129–140.
[88] K.G. Azzam, I.V. Babich, K. Seshan, L. Lefferts, J. Catal. 251 (2008) 163–171.
[89] I.D. González, R.M. Navarro, M.C. Álvarez-Galván, F. Rosa, J.L.G. Fierro, Catal. Commun. 9 (2008) 1759–1765.
[90] T. Takeguchi, S. Manabe, R. Kikuchi, K. Eguchi, T. Kanazawa, S. Matsumoto, W. Ueda, Appl. Catal. A: Gen. 293 (2005) 91–96.
[91] H.C. Yao, Y.F. Yu Yao, J. Catal. 86 (1984) 254–265.